# Measurement report: Variations and environmental impacts of atmospheric $N_2O_5$ concentrations in urban Beijing during the 2022 Winter Olympics

Tiantian Zhang[1], Peng Zuo[2], Yi Chen[2], Tong Liu[1], Linghan Zeng[2], Weili Lin[1,3*], Chunxiang Ye [2*]

[1]NEAC Key Laboratory of Ecology and Environment in Minority Areas, College of Life and Environmental Sciences, Minzu University of China, Beijing, 100081, China

[2]State Key Joint Laboratory for Environmental Simulation and Pollution Control, College of Environmental Sciences and Engineering, Peking University, Beijing, 100871, China

[3]Institute of National Security, Minzu University of China, Beijing, 100081, China

*Correspondence to*: Weili Lin (linwl@muc.edu.cn) and Chunxiang Ye (c.ye@pku.edu.cn)

**Abstract.** The chemistry of nitrate radical ($NO_3$) and dinitrogen pentoxide ($N_2O_5$) plays a pivotal role in tropospheric nighttime chemistry. Given their close linkage to precursor variations, emission reduction during the 2022 Beijing Winter Olympics likely affected $NO_3$ and $N_2O_5$ behavior. In this study, we measured $N_2O_5$, $NO_2$, $O_3$, etc. during and after the Olympics, and compared pollutant levels as well as the contributions of reaction pathways to the loss of $NO_3$ and $N_2O_5$. Throughout the entire observation period, $NO_3$ production rate averaged 0.5 ± 0.4 ppbv $h^{-1}$, and the $N_2O_5$ mixing ratio could reach up to 875 pptv within 1 minute, indicating their active production. The relatively long nighttime $N_2O_5$ lifetime ($\tau_{N_2O_5}$), with an average of 11.9 ± 11.8 minutes, suggested a slow $N_2O_5$ loss rate during winter season. Despite low NO mixing ratio (below 3 ppbv), it dominated $NO_3$ loss (79.0%). VOCs oxidation contributed 0.2%, primarily driven by styrene. During the Olympics, emission reductions led to decreased NO and VOCs, which in turn reduced their reaction with $NO_3$. The heterogeneous uptake of $N_2O_5$, another key $NO_3$ loss pathway—accounted for 20.8% of $NO_3$ loss during the Olympics, but this contribution decreased to 10.6% after the Olympics. This uptake is crucial for nighttime $NO_3$ removal and would be essential for winter nitrate formation in urban Beijing. Our results highlight that under emission control scenarios, the relative importance of heterogeneous processes in nocturnal $NO_3$ cycling increases, providing new insights into how emission reduction measures shape nighttime oxidation processes in polluted urban environments.

## 1 Introduction

Nitrate radical ($NO_3$) and dinitrogen pentoxide ($N_2O_5$) play crucial roles in the nocturnal atmospheric chemical cycle, controlling the removal and conversion of nitrogen oxides ($NO_x$) and volatile organic compounds (VOCs). They significantly contribute to the formation of nitrate and secondary organic aerosols during the nighttime (Crutzen, 1979; Wayne et al., 1991). $NO_3$ primarily originates from the reaction of $NO_2$ with $O_3$ (R1), while it rapidly establishes a thermodynamic equilibrium (R2) with $N_2O_5$. This tight coupling species are frequently considered simultaneously in atmospheric chemistry studies. During daytime, however, the rapid photolysis of $NO_3$ (R3) and its reaction with NO (R4) result in a short $NO_3$ lifetime (< 5 s). Consequently, the concentrations of $NO_3$ and $N_2O_5$ usually fall below the detection limit of analytical instruments during daylight hours.

The direct removal pathways of $NO_3$ include heterogeneous reactions on particulate matter surfaces and gas-phase reactions with NO (R4) and VOCs (R5), which can influence the atmospheric lifetimes of nighttime $NO_x$ and VOCs (Ng et al., 2017; Wayne et al., 1991). $NO_3$ is also capable of reacting with alkenes in an addition reaction (R5) and subsequently with $O_2$ to form peroxy radicals ($RO_2$), which further generates organic nitric acid, one of the important sources of secondary organic aerosols (Fry and Sackinger, 2012; Hoyle et al., 2007; Pye et al., 2010). The removal pathways of $N_2O_5$ represent indirect removal pathways for $NO_3$ chemistry (R6), primarily involving reactions with water vapor and heterogeneous reactions on cloud droplets or particle surfaces (Brown and Stutz, 2012; Chang et al., 2011).

$$NO_2 + O_3 \rightarrow NO_3 + O_2 \quad \text{(R1)}$$

$NO_2 + NO_3 \leftrightarrows N_2O_5$ (R2)

$NO_3 + hv \rightarrow O_2 + NO$ (R3)

$NO_3 + NO \rightarrow 2NO_2$ (R4)

$NO_3 + VOC \rightarrow$ products (R5)

$N_2O_5 + H_2O\ (l) \rightarrow 2HNO_3$ (R6)

In recent years, anthropogenic emission control measures have played a pivotal role in improving air pollution in China with notable declines in $NO_x$ emissions (Li et al., 2020; Zhang et al., 2016). However, $NO_x$ emission intensity remains relatively high (Li et al., 2024). Reactive nitrogen-containing compounds have emerged as a prominent factor in China's complex air pollution scenario (Zhu et al., 2023). With advancements in measurement techniques, several research teams have explored the core processes of reactive nitrogen species in atmospheric pollution, particularly in regions with severe atmospheric pollution such as the North China Plain, the Yangtze River Delta, and the Pearl River Delta (Li et al., 2020; Tham et al., 2016; Wang et al., 2018, 2020, 2024, 2013; Yun et al., 2018). While $NO_3$ reactivity is typically attenuated under low-temperature winter conditions, thereby restricting its oxidative capacity, multiple studies—including winter campaigns such as Yun et al., (2018) and Yan et al., (2023)—have demonstrated the significance of nocturnal $NO_3$ chemistry in cold seasons.

Emerging evidence further highlights the sensitivity of nocturnal $NO_3$ chemistry to emission controls: increases in nocturnal $NO_3$ production rates enhance nighttime oxidation capacity (Wang et al., 2023a), and urban nocturnal $NO_3$ concentrations may even experience “explosive” growth under stringent emission reduction policies (Wang et al., 2023b). In the Beijing region specifically, Yan et al., (2023) showed that the contribution of nocturnal nitrogen chemistry to winter haze has increased in recent years. Despite these advances, gaps remain in our understanding how short-term, large-scale emission control measures—such as those implemented during major events—influence the balance between $NO_3/N_2O_5$ production and loss, and their subsequent impacts on nighttime secondary pollution.

The 2022 Beijing Winter Olympics (BWO) provided a unique opportunity to address this gap. To ensure high air quality during the event, a series of strict emission reduction measures were implemented in Beijing and its surrounding areas, leading to a significant decline in $PM_{2.5}$ concentrations (average 24 μg $m^{-3}$) compared to historical levels for the same period (Huang et al., 2024). Given the close linkage between $NO_3/N_2O_5$ and their precursors ($NO_2$, $O_3$, and VOCs), this emission cuts were expected to alter the behavior of $NO_3$ and $N_2O_5$.

In this study, we conducted field observations of $N_2O_5$, $NO_2$, $O_3$, NO, VOCs, and meteorological parameters in urban Beijing during (5–20 February 2022) and after (21 February–3 March 2022) the BWO. Our objectives

were to: (1) characterize the temporal variations of $N_2O_5$ and $NO_3$ in urban Beijing during winter; (2) quantify the contributions of different reaction pathways to $NO_3$ and $N_2O_5$ loss; and (3) assess how the BWO emission reduction measures modulated nocturnal $NO_3/N_2O_5$ chemistry. The findings provide critical insights into the response of nighttime reactive nitrogen chemistry to short-term emission controls, with implications for air quality management in polluted urban environments.

## 2 Methods

### 2.1 Site description

Field measurements were conducted from 5 February to 3 March 2022 at an urban site in Beijing. The observation location was situated on the rooftop of the NO. 1 Science Building at Peking University in Beijing (39.99° N, 116.31° E, 61.6 m asl). As shown in Figure 1, the location is proximal to the North Fourth Ring Road—one of Beijing's major traffic arteries—and within 1 km of two primary traffic corridors (east-west along the North Fourth Ring Road and north-south along Zhongguancun Street). The surrounding area features mixed land use, including residential complexes (within 500 m) and low-intensity commercial facilities (within 1 km), with no large industrial sources within a 5 km radius. This setting makes the site representative of a typical urban mixed-use area impacted by fresh anthropogenic emissions (e.g., traffic-related $NO_x$ and VOCs), consistent with previous characterizations of this location (Hu et al., 2023; Wang et al., 2017a; Yao et al., 2023).

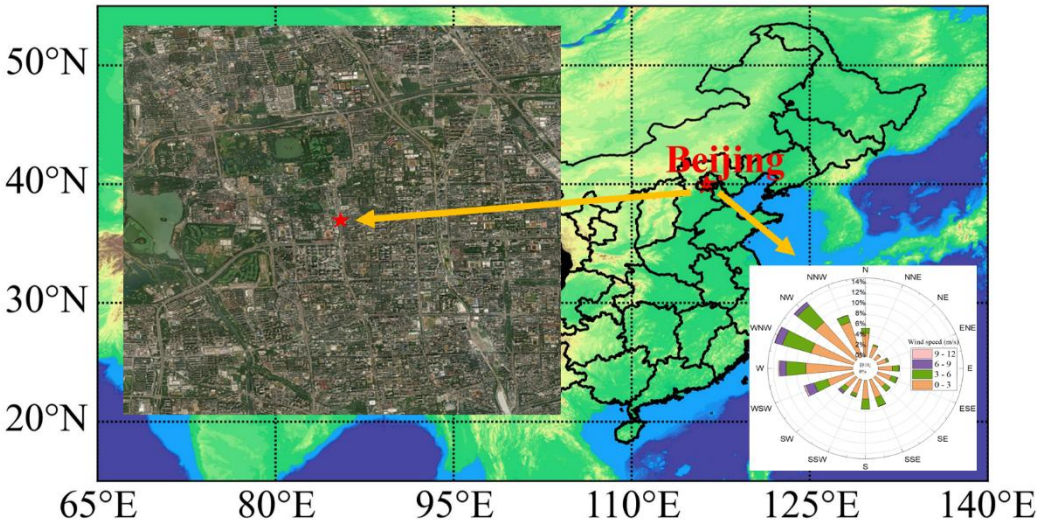


**Figure 1. Measurement site, surroundings, and wind rose (winter 2022). Base map adapted from https://map.baidu.com/); wind rose generated from on-site meteorological observations.**

Sampling inlets were installed 1.5 meters above the rooftop, approximately 20 meters above ground level. Throughout the measurement period, the prevailing wind direction was predominantly from the northwest, with an average wind speed of 2.0 ± 2.0 m $s^{-1}$.

## 2.2 Instrument setup

### 2.2.1 Measurement of $NO_3$ and $N_2O_5$

Ambient concentrations of $NO_3$ and $N_2O_5$ were determined utilizing an in-house-developed cavity ring-down spectroscopy (CRDS) analyzer, operating at a wavelength of 662 nm (Zhang et al., 2024). The analyzer employs a dual-channel design for simultaneous detection: Channel 1 directly measures $NO_3$ concentrations under ambient temperature conditions; Channel 2 maintained at 150 °C to thermally decompose $N_2O_5$ into $NO_3$, enabling quantification of the total concentration of [$NO_3$ + $N_2O_5$].

During this observation campaign, the $NO_3$-specific detection channel (Channel 1) malfunctioned due to the damage of the mirror, limiting measurements to the combined [$NO_3$ + $N_2O_5$] signal from Channel 2. $NO_3$ concentrations were subsequently derived using the thermodynamic equilibrium relationship between $NO_3$ and $N_2O_5$ (Eq. (1) in Section 2.3), with input parameters including measured $N_2O_5$, $NO_2$ concentrations, and ambient temperature. Under winter conditions (low temperature and relatively high $NO_2$ levels), the $NO_3/N_2O_5$ ratio is inherently low (~1%), ensuring that [$NO_3$ + $N_2O_5$] is dominated by $N_2O_5$ and derived $NO_3$ concentrations are reliable.

The limit of detection (LOD) of the CRDS system was calculated as 2.9 pptv, with a measurement uncertainty of ±13.7% (Zhang et al., 2024). To ensure measurement accuracy, regular calibrations were performed using a stable dynamic generation system for $NO_3$ and $N_2O_5$ standard gases (Zhang et al., 2026). The detailed technical specifications of the instrument are provided in Text S1 of the Supporting Information.

### 2.2.2 Measurement of other species

Concentrations of NO, $NO_2$, $O_3$, VOCs, and meteorological parameters were measured using commercial or well-validated analytical instruments, with details summarized in Table 1. NO and $O_3$ mixing ratios were measured using commercial instruments, specifically the Model 42i-Y and Model 49i from Thermo Fisher Scientific (USA). $NO_2$ mixing ratios were observed via a cavity-enhanced absorption spectroscopy (CEAS) (Zhou et al., 2022). Calibrations of these instruments are performed weekly using the standard gases of known concentrations, and the $R^2$ of the standard curve for each calibration is greater than 0.99. VOC concentrations were determined using a gas chromatograph equipped with mass spectrometry and flame ionization detectors (Wang et al., 2014). This system measures 99 VOC species with a time resolution of 1 hour, LOD range of 1–26 pptv, and accuracy of 0.8–6.1%. Quality control included weekly zero/span checks (using ultra-high-purity nitrogen and a multi-component VOC standard) and a post-campaign full calibration, which confirmed linearity ($R^2 > 0.996$) and negligible intercepts for all target VOCs. The photolysis rate constants (*j*-values) were obtained using a spectroradiometer (Metcon CCD-Spectrograph, Garmisch-Partenkirchen, Germany) (Bohn et al., 2008). This instrument quantifies two primary photolysis channels ($NO_3$ + hv → $NO_2$ + $O(^3P)$ and $NO_3$ + hv → NO + $O_2$), with total $j(NO_3)$ calculated as the sum of the two channel-specific rate constants ($j(NO_3)$_total = $j(NO_3)$_M

+ $j(NO_3)$_R). Meteorological parameters, including wind direction, wind speed, temperature ($T$), and relative humidity (RH), were monitored utilizing a sensor meteorological measurement system (Metone, USA). The $PM_{2.5}$ concentration data were obtained from the Beijing Municipal Ecological and Environmental Monitoring Center (bjmemc.com.cn). Detailed information about these instruments is listed in Table 1.

**Table 1 Species measured in the field work**

| Species | Time resolution (s) | Limit of Detection/working range | Methods | Accuracy (%) | References |
|---|---|---|---|---|---|
| $O_3$ | 60 | 1 ppbv (parts per billion by volume) | UV photometry | ± 1 % | - |
| $NO_2$ | 30 | 8 pptv | CEAS | ＜ 6 % | (Zhou et al., 2022) |
| NO | 60 | 50 pptv | chemiluminescence | ± 1 % | - |
| $N_2O_5$ | 60 | 2.9 pptv | CRDS | ± 18 % | (Zhang et al., 2024) |
| VOCs | 3600 | 1–26 pptv | GC-MS/FID | 0.8 % – 6.1 % | (Wang et al., 2014) |
| T | 60 | -50–50℃ | A three-element composite thermistor | ± 0.1℃ | www.metone.com |
| RH | 60 | 0–100 % | Thin film polymer capacitor | ± 0.2 % | www.metone.com |

### 2.3 Calculation methods

When $N_2O_5$ concentrations are obtained, the concentration of $NO_3$ can be determined by dividing the concentration of $N_2O_5$ by the equilibrium constant $K_{eq}$ and the concentration of $NO_2$ (Osthoff et al., 2006; Wang et al., 2017b), which is specified in Eq. (1).

$$[NO_3]=\frac{[N_2O_5]}{K_{eq}[NO_2]} \quad (1)$$

Here, $K_{eq}$ represents the temperature-dependent equilibrium constant established when $NO_3$ attains steady-state equilibrium with $N_2O_5$, and is given by $5.50\times10^{-27}\times \exp(10724/T)$, where $T$ is the temperature in Kelvin (Wang et al., 2024).

The primary source of $NO_3$ and $N_2O_5$ is the chemical reaction of $NO_2$ with $O_3$. Consequently, the concentrations of $NO_2$ and $O_3$ are key factors influencing the production rate of $NO_3$ ($P(NO_3)$). This production rate is mathematically represented by Eq. (2) (Brown et al., 2011). Assuming that the formation and loss processes of $NO_3$ and $N_2O_5$ are in a state of dynamic equilibrium, the lifetime of $N_2O_5$, denoted as $\tau_{N_2O_5}$, can be expressed as the ratio of its concentration to the rate of $NO_3$ production, as determined by Eq. (3) (Brown and Stutz, 2012;

Lin et al., 2022; Wang et al., 2017a).

$$P(NO_3) = k_{NO_2+O_3} \times [NO_2] \times [O_3] \quad (2)$$

$$\tau_{N_2O_5} = \frac{[N_2O_5]}{P(NO_3)} = \frac{[N_2O_5]}{k_{NO_2+O_3} \cdot [NO_2] \cdot [O_3]} \quad (3)$$

The total reactivity of $NO_3$ ($k_{NO_3}$) represents the sum of all first-order loss processes for $NO_3$, including photolysis, reaction with NO, reaction with VOCs, and indirect loss via $N_2O_5$ heterogeneous uptake. It is calculated using Eq. (4)(Wang et al., 2020): The nocturnal $NO_3$ loss rate, denoted as $L(NO_3)$, is calculated via Eq. (5).

$$k_{NO_3} = j(NO_3) + k_{NO_3+NO} \cdot [NO] + k_{NO_3+VOCi} \cdot [VOCi] + k_{N_2O_5} \cdot K_{eq} \cdot [NO_2] \quad (4)$$

$$L(NO_3) = \sum k_i [VOC_i] \cdot [NO_3] + k_{NO_3+NO} \cdot [NO][NO_3] + k_{N_2O_5} \cdot [N_2O_5] \quad (5)$$

Here, $j(NO_3)$ denotes the photolysis rate constant for $NO_3$ decomposition. The rate coefficients $k_{NO_2+O_3}$ and $k_{NO_3+NO}$ correspond to the rate coefficients for reaction Eqs. (1) and (4), respectively, as referenced in Atkinson et al., (2004). The reactivity of $NO_3$ with VOCs ($k_{NO_3+VOCi}$) is characterized by a first order loss rate constant, calculated as the product of the reaction rate constant $k_i$ and the VOC concentrations [$VOC_i$].

$k_{N_2O_5}$ represents the total first-order loss rate coefficient for the heterogeneous uptake of $N_2O_5$ at the aerosol surface, which is governed by the uptake coefficient $\gamma(N_2O_5)$, the aerosol surface area density $S_a$ ($\mu m^2\ cm^{-3}$), and the mean molecular speed of $N_2O_5$, c, as described in Eq. (6).

$$k_{N_2O_5} = \frac{1}{4} c S_a \gamma(N_2O_5) \quad (6)$$

The mean molecular speed c is calculated as $\sqrt{8RT/(\pi M)}$, where R is the gas constant (8.314 J $mol^{-1}$ $K^{-1}$), T is temperature (K), and M is the molar mass of $N_2O_5$ (0.108 kg $mol^{-1}$). $\gamma(N_2O_5)$ is a critical parameter describing the efficiency of $N_2O_5$ uptake on aerosol surfaces, influenced by aerosol composition (e.g., organic coatings, nitrate/sulfate content) and meteorological conditions (RH, temperature) (Bertram et al., 2009; Tang et al., 2014; Yu et al., 2020). It was determined using the steady-state method (Brown et al., 2016; Lin et al., 2022; Lu et al., 2022), which relies on linear regression of $K_{eq}[NO_2]\tau(N_2O_5)^{-1}$and $\frac{1}{4} c S_a K_{eq}[NO_2]$ (Eq. (7)).

$$K_{eq}[NO_2]\ \tau(N_2O_5)^{-1} = \frac{1}{4} c S_a \gamma(N_2O_5)\ K_{eq}[NO_2] + k_{NO_3} \quad (7)$$

Here, the slope of the regression equals $\gamma(N_2O_5)$, and the intercept equals $k_{NO_3}$. To minimize interference from non-steady-state conditions, data fitting was data fitting was performed under the following constraints:

(1) Meteorological constraint: RH < 70% (avoiding excessive water vapor interference); (2) Chemical constraints: NO < 1 ppbv (suppressing NO-$NO_3$ titration), [$N_2O_5$] > LOD (2.9 pptv, ensuring reliable equilibrium calculations); (3) Timing constraint: Data selected 2–3 hours post-sunset (when the $NO_3$-$N_2O_5$ equilibrium is most stable). Negative intercepts (physically implausible, arising from $k_{NO_3}$ ) were excluded, resulting in 23 valid data points for $\gamma(N_2O_5)$ calculation.

**Aerosol surface area density ($S_a$)**

Due to the unavailability of direct particle size distribution measurements, $S_a$ was derived from $PM_{2.5}$ concentrations using an empirical formula validated for winter Beijing conditions (Zhang et al., 2022):

$$S_a = 60.03 \times [PM_{2.5}]^{0.62} \quad (8)$$

This formula exhibits a strong linear correlation ($R^2$ = 0.82) with $PM_{2.5}$ and is applicable for $PM_{2.5}$ concentrations < 200 μg $m^{-3}$—consistent with the $PM_{2.5}$ range observed in this study (average: 24 ± 21 μg $m^{-3}$, maximum: 131 μg $m^{-3}$).

## 3 Results

### 3.1 Measurements overview

Figure 2 illustrates time-series variations in the mixing ratios of $N_2O_5$ and associated trace gases, alongside meteorological parameters, captured during the 2022 Beijing Winter Olympics (BWO) at a temporal resolution of 1 minute. Valid data were systematically acquired over a 26-day span, from 5 February to 3 March. In alignment with the 2022 Beijing Winter Olympics timeline, the observation interval was bifurcated into two distinct periods: (1) the Olympic Games Period (OGP; spanning 5-20 February), and (2) the Post-Olympics Period (POP; extending from 21 February to 3 March). Comprehensive statistical metrics for each period are meticulously detailed in Table 2.

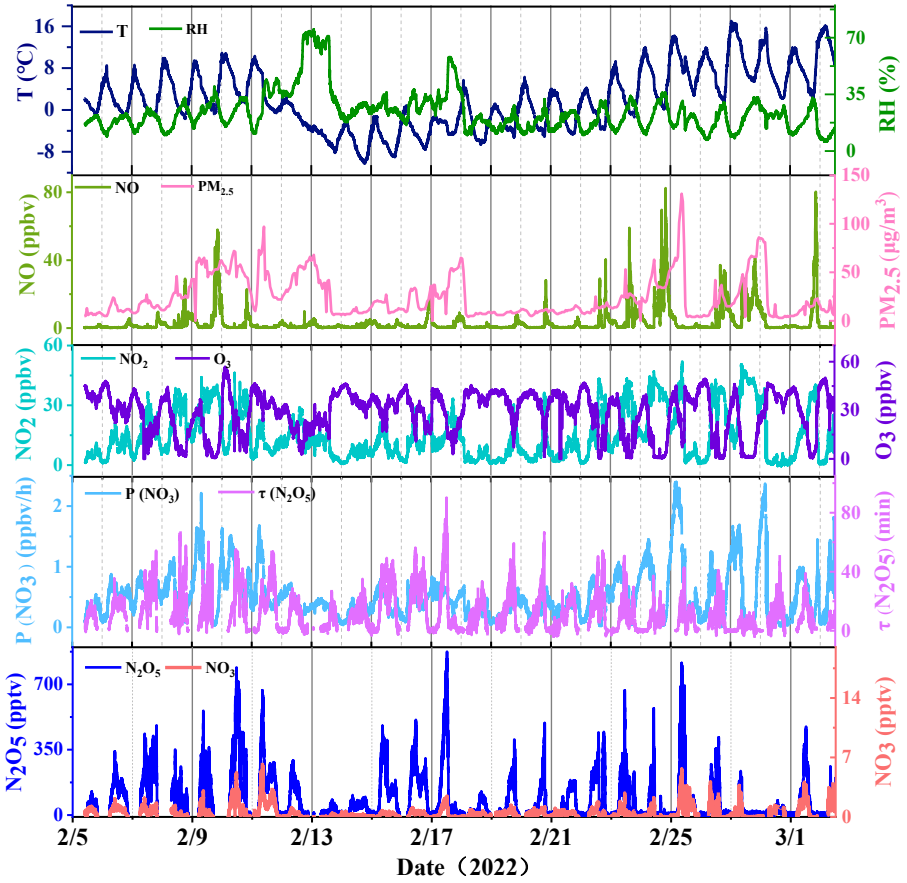


**Figure 2. Time series for $N_2O_5$, $NO_3$, related trace gases, and meteorological data (T and RH) measured in Beijing from 5 February to 3 March 2022.**

### 3.1.1 Meteorological conditions and $PM_{2.5}$

Meteorological conditions differed notably between the OGP and POP, driving variations in pollutant dispersion and chemical reactivity:

**Temperature**: Nocturnal temperatures during the OGP were predominantly below freezing (average: -1.4 ± 3.6 °C), while the POP saw a marked warming trend—nocturnal temperatures rose to 3.5 ± 3.5 °C (all-day average: 5.6 ± 3.9 °C, vs. -0.4 ± 3.9 °C in the OGP).

**Relative Humidity (RH)**: The OGP exhibited higher RH (nocturnal average: 29 ± 13%) compared to the POP (nocturnal average: 20 ± 4 %). A heavy snowfall event occurred during 13–14 February (OGP), coinciding with peak RH (> 60%) and a transient increase in $PM_{2.5}$ concentration (68 μg $m^{-3}$).

**$PM_{2.5}$:** The overall average $PM_{2.5}$ concentration across the entire observation period was 24 ± 21 μg $m^{-3}$, consistent with the improved air quality during the BWO (Huang et al., 2024). While $PM_{2.5}$ levels were similar

between the OGP (nocturnal average: 26 ± 2 μg $m^{-3}$) and POP (nocturnal average: 23 ± 2 μg $m^{-3}$), the POP experienced a severe pollution episode with $PM_{2.5}$ peaking at 131 μg $m^{-3}$—likely driven by relaxed emissions and stagnant meteorological conditions.

The aerosol surface area density, a key parameter for $N_2O_5$ heterogeneous uptake calculations (Eq. (8)), was derived from $PM_{2.5}$ concentrations. The overall average $S_a$ was 402 ± 215 $\mu m^2$ $cm^{-3}$, with values in the OGP (nocturnal average: 417 ± 208 $\mu m^2$ $cm^{-3}$) slightly higher than in the POP (nocturnal average: 385 ± 205 $\mu m^2$ $cm^{-3}$), reflecting the influence of $PM_{2.5}$ and RH-driven aerosol growth.

**Table 2. Summary of observed parameters for the two periods (mean ± standard deviation).**

| Species | All time | OGP | | POP | |
|---|---|---|---|---|---|
| | | All day | Nighttime | All day | Nighttime |
| $O_3$ (ppbv) | 28.6 ± 12.8 | 29.9 ± 9.5 | 27.4 ± 10.3 | 26.7 ± 10.6 | 19.8 ± 12.1 |
| $NO_2$ (ppbv) | 14.8 ± 11.5 | 12.6 ± 8.2 | 14.5 ± 9.3 | 18.2 ± 12.3 | 20.7 ± 13.1 |
| NO (ppbv) | 3.5 ± 7.2 | 1.9 ± 2.3 | 1.0 ± 1.2 | 5.7 ± 6.1 | 4.8 ± 6.0 |
| $N_2O_5$ (pptv) | 86.7 ± 116.5 | 87.3 ± 71.6 | 137.6 ± 112.7 | 62.1 ± 57.7 | 97.8 ± 90.3 |
| $NO_3$ (pptv) | 0.6 ± 0.7 | 0.4 ± 0.4 | 0.6 ± 0.6 | 0.3 ± 0.4 | 0.5 ± 0.6 |
| Total VOCs (ppbv) | 17.36±10.10 | 15.67 ± 7.45 | 16.02 ± 7.74 | 19.72 ± 11.93 | 19.68 ± 12.17 |
| $PM_{2.5}$ (μg $m^{-3}$) | 24 ± 21 | 25 ± 2 | 26 ± 2 | 23 ± 3 | 23 ± 2 |
| T (°C) | 2.1 ± 5.7 | -0.4 ± 3.9 | -1.4 ± 3.6 | 5.6 ± 3.9 | 3.5 ± 3.5 |
| RH (%) | 24 ± 12 | 27 ± 13 | 29 ± 13 | 19 ± 4 | 20 ± 4 |
| $P(NO_3)$ (ppbv $h^{-1}$) | 0.5 ± 0.4 | 0.5 ± 0.2 | 0.5 ± 0.2 | 0.6 ± 0.4 | 0.5 ± 0.3 |
| $\tau_{N_2O_5}$ (min) | 11.9 ± 11.8 | 10.9 ± 17.0 | 17.0 ± 17.0 | 7.4 ± 4.4 | 11.6 ± 6.8 |

### 3.1.2 Precursor gases (NO, $NO_2$, $O_3$)

Concentrations of $NO_x$ (NO + $NO_2$) and $O_3$—key precursors for $NO_3/N_2O_5$ production (Reaction R1)—exhibited distinct differences between the OGP and POP, directly reflecting the impact of emission controls:

**NO**: The OGP observed significantly lower NO concentrations compared to the POP—nocturnal NO averaged 1.0 ± 1.2 ppbv (OGP) vs. 4.8 ± 6.0 ppbv (POP). This contrast confirms BWO emission reductions effectively curbed primary NO emissions (e.g., traffic, industry), which further modulated $O_3$ and $NO_2$ dynamics.

**$NO_2$**: Inverse to NO, $NO_2$ concentrations were higher in the POP. Nocturnal $NO_2$ averaged 20.7 ± 13.1 ppbv in the POP, compared to 14.5 ± 9.3 ppbv in the OGP. The increase in $NO_2$ during the POP is attributed to enhanced NO oxidation by $O_3$, driven by higher post-Olympic NO emissions.

**$O_3$:** Nocturnal $O_3$ levels were substantially higher in the OGP (27.4 ± 10.3 ppbv) than in the POP (19.8 ± 12.1 ppbv), despite similar all-day averages (OGP: 29.9 ± 9.5 ppbv; POP: 26.7 ± 10.6 ppbv). The lower nocturnal $O_3$ in the POP results from intensified $O_3$ titration by elevated NO, a process that simultaneously increases $NO_2$ concentrations. Notably, the overall mean $O_3$ concentration (28.6 ± 12.8 ppbv) was lower than spring values in Beijing (Wang et al., 2018), consistent with reduced photochemical $O_3$ production in winter.

The average $NO_x$ concentration (18.2 ± 16.6 ppbv) during the study was also substantially lower than autumn values at this site (typically > 30 ppbv) (Li et al., 2022; Wang et al., 2017a), further highlighting the effectiveness of winter emission controls.

### 3.1.3 $N_2O_5$ and $NO_3$ concentrations

$N_2O_5$ concentrations exhibited significant temporal variability throughout the observation period, with a mean daily value of 86.7 ± 116.5 pptv and a maximum of 874.9 pptv (00:15 LST on 18 February, OGP)—coinciding with moderate $NO_2$ (14.6 ppbv)、$O_3$ (26.8 ppbv) and extremely low NO (0.4 ppbv) that minimized $NO_3$ titration.

$NO_3$ concentrations were derived from the $NO_3$-$N_2O_5$ equilibrium (Eq. (1)), with a mean value of 0.6 ± 0.7 pptv (maximum: 4.6 pptv). Nocturnal $NO_3$ levels followed the same trend as $N_2O_5$: higher in the OGP (0.6 ± 0.6 pptv) than in the POP (0.5 ± 0.6 pptv). This derived $NO_3$ concentration is notably lower than observations in Shanghai (16 ± 9 pptv) (Wang et al., 2013), likely due to Beijing's lower winter temperatures (which suppress $NO_3$ production) and higher NO emissions (which enhance $NO_3$ loss).

### 3.1.4 $NO_3$ production rate and $N_2O_5$ lifetime

The $NO_3$ production rate, calculated via Eq. (2) as the product of the $NO_2$ + $O_3$ reaction rate constant and precursor concentrations, averaged 0.5 ± 0.4 ppbv $h^{-1}$ across the entire observation period, with a maximum of 2.4 ppbv $h^{-1}$. This value aligns with winter observations in the Beijing area (0.4 ppbv $h^{-1}$) (Wang et al., 2021) and summer measurements at Mount Tai (0.45 ± 0.40 ppbv $h^{-1}$) (Wang et al., 2017c), but is lower than autumn values in Beijing (2.25 ± 2.02 ppbv $h^{-1}$) (Wang et al., 2017a) and summer measurements in Taizhou (1.2 ± 0.3 ppbv $h^{-1}$) (Li et al., 2020). The relatively low $P(NO_3)$ in this study is primarily driven by winter's low temperatures, which reduce the $NO_2$ + $O_3$ reaction rate constant: for example, at identical $NO_2$ (15 ppbv) and $O_3$ (30 ppbv) concentrations, increasing temperature from -1 °C to 5 °C raises the rate constant from $1.59\times10^{-17}$ to $1.94\times10^{-17}$ $cm^3$ $molecule^{-1}$ $s^{-1}$, leading to a 19% increase in $P(NO_3)$ (from 0.70 to 0.83 ppbv $h^{-1}$).

The $N_2O_5$ lifetime, a key indicator of $N_2O_5$ removal efficiency (Eq. (3)), averaged 11.9 ± 11.8 minutes across the study—longer than summer values in Beijing (270 ± 240 seconds) (Wang et al., 2018)and rural Wangdu (77–172 seconds) (Tham et al., 2016), but shorter than observations in the Hong Kong boundary layer (Brown et al., 2016). This prolonged winter $\tau_{N_2O_5}$ suggests slower nocturnal $NO_3$/$N_2O_5$ loss, consistent with lower winter temperatures and reduced heterogeneous reactivity.

Notably, $\tau_{N_2O_5}$ differed significantly between the OGP and POP: the nocturnal mean lifetime was 17.0 ± 17.0 minutes in the OGP, compared to 11.6 ± 6.8 minutes in the POP—a ~5-minute reduction. This difference is primarily driven by variations in $N_2O_5$ concentrations (rather than $P(NO_3)$, which was similar between periods: OGP nocturnal $P(NO_3)$ = 0.5 ± 0.2 ppbv $h^{-1}$; POP = 0.5 ± 0.3 ppbv $h^{-1}$).

### 3.2 Mean diurnal variations

Figure 3 displays the average diurnal variations in NO, $NO_2$, $N_2O_5$, $NO_3$, $O_3$ mixing ratios, and $P(NO_3)$ during the study period. Specifically, panel (a) presents the daily mean patterns for the OGP, whereas panel (b) depicts those for the POP. Notable differences in concentration but similar diurnal trends were observed between the two periods.

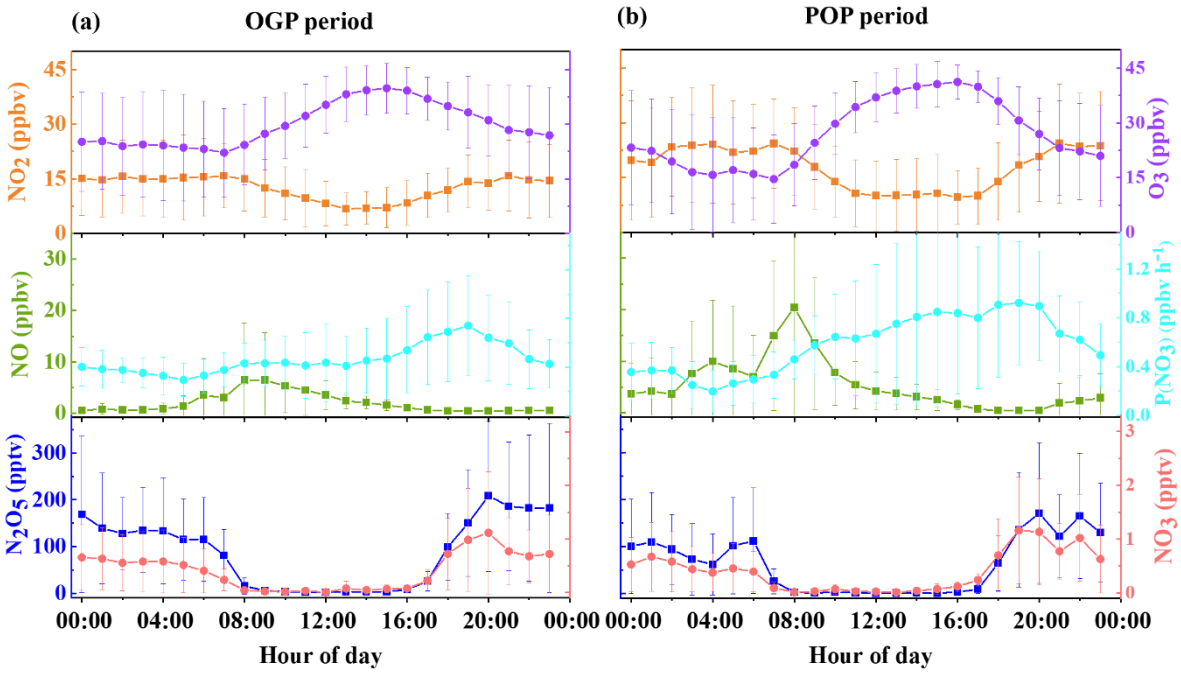


**Figure 3. Mean diurnal variations in NO, $NO_2$, $N_2O_5$, $NO_3$, $O_3$ mixing ratios and $P(NO_3)$ during (a) the Olympic Games Period (OGP) and (b) the Post-Olympics Period (POP). Data represent hourly means with error bars indicating the standard deviation; non-physical values < 0 (for $NO_3$) have been excluded.**

#### 3.2.1 Diurnal cycles of precursor gases (NO, $NO_2$, $O_3$)

The diurnal variations of NO, $NO_2$, and $O_3$ exhibit strong interdependencies, consistent with well-documented atmospheric chemical processes (e.g., $O_3$ titration by NO, $NO_2$ photolysis) and anthropogenic emission patterns.

Nocturnal NO mixing ratios were substantially lower in the OGP than in the POP, with OGP nighttime values remaining below 2 ppbv (average: 1.0 ± 1.2 ppbv) and POP values frequently exceeding 4 ppbv (average: 4.8 ± 6.0 ppbv). Both periods showed two distinct daily peaks in NO, aligned with morning (06:00–08:00 LST)

and evening (18:00–20:00 LST) traffic rush hours—confirming traffic as the primary NO source. The morning peak was particularly pronounced in the POP, reaching 20.4 ppbv at 08:00 LST (vs. 6.4 ppbv at 06:00 LST in the OGP), directly attributable to relaxed post-Olympic traffic emission controls.

$NO_2$ concentrations displayed an inverse diurnal trend to $O_3$, with nocturnal levels consistently higher than daytime values (OGP: 14.5 ± 9.3 ppbv nighttime vs. 12.6 ± 8.2 ppbv all-day; POP: 20.7 ± 13.1 ppbv nighttime vs. 18.2 ± 12.3 ppbv all-day). This pattern arises from reduced daytime $NO_2$ photolysis ($NO_2 + hv \rightarrow NO + O$) and enhanced nocturnal NO oxidation. The POP saw higher $NO_2$ concentrations across all hours, with the nocturnal peak (24.3 ppbv at 21:00 LST) exceeding the OGP peak (15.9 ppbv at 21:00 LST) by ~35%—a result of elevated NO emissions driving more $O_3$-to-$NO_2$ conversion.

$O_3$ exhibited a classic mid-afternoon peak in both periods, rising gradually after sunrise (07:00 LST) as photochemical production intensified, and peaking between 15:00–16:00 LST (OGP: 39.9 ppbv; POP: 41.2 ppbv). Nocturnal $O_3$ levels, however, differed sharply: the OGP maintained higher nighttime $O_3$ (27.4 ± 10.3 ppbv) compared to the POP (19.8 ± 12.1 ppbv), with the POP $O_3$ concentration dropping to a minimum of 14.6 ppbv at 07:00 LST (vs. 22.2 ppbv in the OGP). This discrepancy stems from intensified $O_3$ titration by NO in the POP—higher NO concentrations rapidly consume $O_3$ via $NO + O_3 \rightarrow NO_2 + O_2$, reducing the $O_3$ pool available for $NO_3$ production (Reaction R1).

### 3.2.2 Diurnal cycles of $NO_3$ production rate

$P(NO_3)$ exhibited a strong diurnal pattern tied to the availability of its precursors ($NO_2$ and $O_3$) and the suppression of daytime $NO_3$ loss.

In both periods, $P(NO_3)$ peaked shortly after sunset (19:00 LST), when $O_3$ concentrations remained relatively high (OGP: 33.3 ppbv; POP: 30.6 ppbv) and NO emissions (and thus $NO_3$ titration) were still low. The OGP peak $P(NO_3)$ was 0.74 ppbv $h^{-1}$, slightly lower than the POP peak (0.92 ppbv $h^{-1}$)—a difference driven by the POP's higher $NO_2$ concentrations (18.4 ppbv at 19:00 LST vs. 14.2 ppbv in the OGP) offsetting its lower $O_3$.Throughout the night, $P(NO_3)$ gradually declined in both periods: by 04:00 LST, it dropped to 0.33 ppbv $h^{-1}$ (OGP) and 0.20 ppbv $h^{-1}$ (POP), mirroring the nocturnal decrease in $O_3$.

Notably, $P(NO_3)$ showed a strong first-order exponential decay correlation with NO concentrations (Figure S2): when NO < 5 ppbv, $P(NO_3)$ decreased sharply with increasing NO (from 1.2 ppbv $h^{-1}$ to 0.5 ppbv $h^{-1}$); when NO > 10 ppbv, $P(NO_3)$ stabilized at < 0.3 ppbv $h^{-1}$. This confirms NO is a dominant inhibitor of $NO_3$ production—even small NO increases (e.g., POP rush hours) rapidly consume $NO_3$ as it forms.

### 3.2.3 Diurnal cycles of $N_2O_5$ and $NO_3$

$N_2O_5$ and $NO_3$ exhibited nearly identical diurnal patterns in both periods, reflecting their tight thermodynamic

equilibrium (Reaction R2) and shared dependence on precursor availability and loss pathways:

**Post-sunset accumulation**: Both species began accumulating rapidly after sunset (18:00 LST), as photolysis (a major daytime $NO_3$ loss pathway) ceased. They reached peak concentrations around 20:00 LST—shortly after the $P(NO_3)$ peak—with OGP peaks ($N_2O_5$: 208.2 pptv; $NO_3$: 1.1 pptv) exceeding POP peaks ($N_2O_5$: 171.2 pptv; $NO_3$: 1.0 pptv) by ~22%. This difference is driven by the OGP's lower NO concentrations, which reduce $NO_3$ titration (Reaction R4) and allow more $N_2O_5$ to form via equilibrium.

**Nocturnal decline**: After the 20:00 LST peak, $N_2O_5$ and $NO_3$ concentrations gradually decreased in the OGP, falling to near-detection limits by sunrise (07:00 LST). The POP, however, showed a steeper decline between 02:00–04:00 LST: $N_2O_5$ dropped from 94.1 pptv to 61.8 pptv, and $NO_3$ from 0.6 pptv to 0.3 pptv—attributed to elevated nocturnal NO emissions in the POP (peaking at 9.9 ppbv at 04:00 LST) that accelerate $NO_3$ loss.

**Morning secondary peak (POP only)**: A notable secondary peak in $N_2O_5$ (112.1 pptv at 06:00 LST) and $NO_3$ (0.5 pptv at 06:00 LST) occurred in the POP, coinciding with a transient increase in $O_3$ (1.3 ppbv) and decrease in NO (2.9 ppbv) before morning rush hour. This peak is absent in the OGP, likely because lower POP emission controls led to a larger "pre-rush" $O_3$ pool that drives $NO_3$ production, while OGP NO emissions remained too low to support such a transient precursor balance.

The daily average variation trends of both $N_2O_5$ and $NO_3$ aligned with those reported for the Yangtze River Delta and North China regions (Li et al., 2020; Wang et al., 2022, 2017b). While the chemical conditions in this study bore similarities to those in summer Beijing, the meteorological conditions differed, notably characterized by higher relative humidity during the summer. The average nocturnal $N_2O_5$ concentration over the observation period was 113.7 ± 103.3 pptv, which was higher than that observed in the Changping area of Beijing (Wang et al., 2018), indicating that the loss process of $NO_3$ and $N_2O_5$ in Beijing during winter is more sluggish compared to that in the summer.

## 4 Discussion

### 4.1 Factoring influencing $N_2O_5$ lifetime

RH and $S_a$ are well-recognized as pivotal factors regulating $N_2O_5$ lifetime in nocturnal atmospheric chemistry, as they directly modulate the efficiency of $N_2O_5$ heterogeneous uptake—the primary indirect loss pathway for $NO_3$ (Brown et al., 2017; Lin et al., 2022).The correlation between these parameters and $\tau_{N_2O_5}$ is presented in Figure 4.

#### 4.1.1 Relationship between $\tau_{N_2O_5}$ and RH

As shown in Figure 4(a), the correlation between $\tau_{N_2O_5}$ and RH exhibits a humidity-dependent dual pattern. At RH < 35%, $\tau_{N_2O_5}$ increased with RH—slight humidity rises softened hydrophobic organic coatings on aerosols (from traffic VOC oxidation), thereby reducing $N_2O_5$ heterogeneous uptake. RH > 35%, the heterogeneous uptake rate of $N_2O_5$ increases, and $\tau_{N_2O_5}$ decreases with increasing RH.

**RH < 35%**: Counterintuitive $\tau_{N_2O_5}$ increases with rising RH. Minimal aerosol liquid water content drives hydrophobic organic components—primarily oxidation products of traffic-related anthropogenic VOCs (AVOCs, e.g., styrene, propylene)—to condense into dense, impermeable coatings on particle surfaces (Bertram et al., 2009; Folkers et al., 2003; McNeill et al., 2006; Tang et al., 2014). These coatings act as a diffusion barrier, preventing $N_2O_5$ from reaching reactive aqueous sites (e.g., nitrate/sulfate-rich droplets) and lowering the heterogeneous uptake coefficient $\gamma(N_2O_5)$ (Anttila et al., 2006; Yu et al., 2020). For example, at RH = 25%, $\tau_{N_2O_5}$ averaged 15.5 minutes, 43% longer than the 8.9 minutes observed at RH = 15%.

**RH > 35%**: $\tau_{N_2O_5}$ decreases with increasing RH (conventional trend). Above 35% RH, the relationship aligns with physical expectations: $\tau_{N_2O_5}$ declines as RH increases, driven by two synergistic effects. First, hygroscopic growth of aerosols (e.g., ammonium sulfate, sodium chloride) increases $S_a$, providing more reactive surface sites for $N_2O_5$ uptake. Second, elevated aerosol liquid water content accelerates $N_2O_5$ hydrolysis, which becomes the dominant $N_2O_5$ loss pathway (Brown et al., 2016; Chang et al., 2011). This effect is particularly pronounced when RH > 60%: during the snowfall events on 13–14 February 2022, $\tau_{N_2O_5}$ approached zero (0.8 ± 0.3 minutes), as high RH (> 85%) maximized both aerosol growth and hydrolysis efficiency.

Notably, scattered data points in the 30–40% RH range (e.g., $\tau_{N_2O_5}$ ranging from 2 to 33 minutes at RH = 35%) suggest interference from transient factors—such as sudden NO spikes or shifts in aerosol organic composition—which obscure the RH- $\tau_{N_2O_5}$ relationship. A more comprehensive discussion of these confounding factors requires consideration of the organic composition of the aerosol.

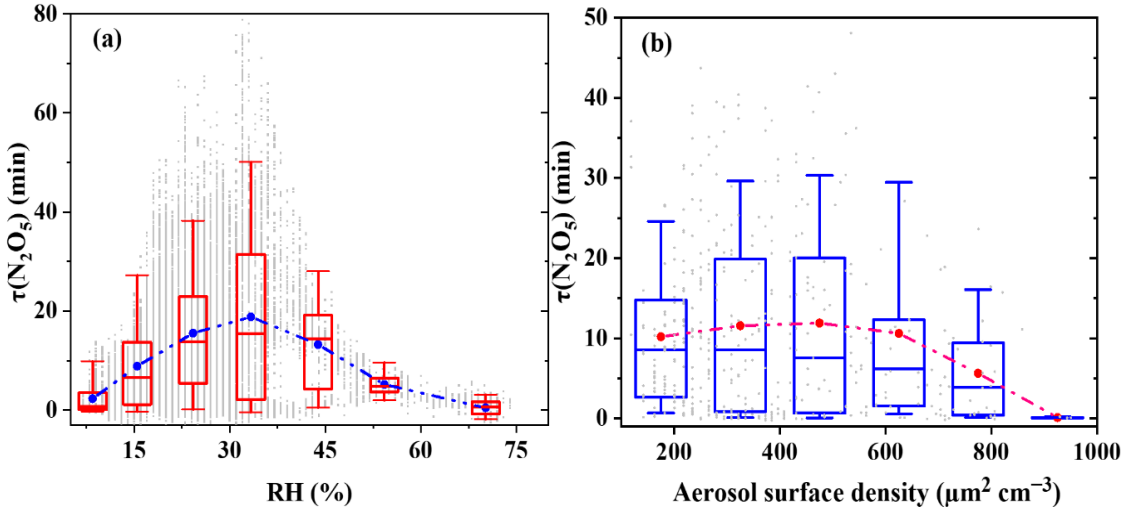

**Figure 4. The relationship between $\tau_{N_2O_5}$ and $S_a$ as well as RH during the observation period.**

#### 4.1.2 Relationship between $\tau_{N_2O_5}$ and $S_a$

Figure 4(b) depicts the dependence of $\tau_{N_2O_5}$ on $S_a$, reflecting the interplay between $S_a$ and other regulating factors (e.g., RH, organic coatings).

**$S_a$ < 325 μm² cm⁻³:** $\tau_{N_2O_5}$ gradually increases with rising $S_a$. For low $S_a$ values, $\tau_{N_2O_5}$ gradually rises from ~10 to 12 minutes as $S_a$ increases. This non-monotonic pattern is driven by the co-occurrence of low $S_a$ with extremely dry conditions (RH < 25% for 68% of data points in this $S_a$ range).

**$S_a$ = 500–1000 μm² cm⁻³:** Robust negative correlation. Above a threshold $S_a$ of ~500 μm² cm$^{-3}$, a clear negative correlation emerges: $\tau_{N_2O_5}$ decreases from ~12 to 6 minutes as $S_a$ increases. This aligns with physical expectations, as higher $S_a$ provides more reactive surface area for $N_2O_5$ heterogeneous uptake(Lin et al., 2022; Wang et al., 2020; Zhou et al., 2018).

Quantitative discrepancies between our results and summer studies (e.g., Zhou et al., 2018 reported $\tau_{N_2O_5}$ < 5 minutes at $S_a$ > 600 μm$^2$cm$^{-3}$in urban Beijing) are attributed to seasonal differences in aerosol liquid water content. Winter's lower RH (average: 24 ± 12%) reduces aerosol liquid water content, lowering $\gamma(N_2O_5)$ and slowing $N_2O_5$ loss—even at high $S_a$. This highlights the need for season-specific parameterizations of $S_a$-$\tau_{N_2O_5}$ relationships in air quality models.

### 4.2 $NO_3$ and $N_2O_5$ loss pathways

To quantify the mechanisms governing $NO_3$ and $N_2O_5$ removal, we calculated total $NO_3$ reactivity via Eq. (4) and dissected the contributions of individual loss pathways. The reaction rate constants for the interaction between VOCs and the oxidizing agent $NO_3$ were obtained from the literature ((Atkinson and Arey, 2003; Brown et al., 2011) or extracted from the National Institute of Standards and Technology database (accessible via http://webbook.nist.gov/chemistry/). For certain VOC species where quantitative laboratory reaction rate constants were unavailable, these values were estimated based on the reaction rate constants of analogous species.

#### 4.2.1 $NO_3$ Loss via VOC oxidation and $N_2O_5$ uptake

VOC-driven $NO_3$ loss is negligible in winter urban Beijing, but distinct patterns emerge in the concentrations and reactivity of different VOC categories. Detailed statistical data regarding VOC concentrations (e.g., styrene, isoprene, and other anthropogenic species) and their corresponding $NO_3$ reaction rates—are provided in Table S1 (auxiliary material). Time series plots of the concentrations of several highly reactive VOCs (Figure S3) show that the styrene concentration peaks at 86 pptv, while the isoprene concentration peaks at 96 pptv.

Comparative analysis reveals these high-VOC periods coincide with enhanced NO (e.g., NO spikes to 24.8 ppbv on February 24, POP), suggesting VOCs and NO share a common emission source (traffic exhaust)—consistent with the site's proximity to urban traffic corridors (Section 2.1).

**High-concentration AVOCs contribute minimally.** The most abundant VOCs—ethane (3.8 ± 1.8 ppbv), propane (2.1 ± 1.3 ppbv), and acetone (1.4 ± 0.8 ppbv)—exhibit extremely low $k_{NO_3}$ (e.g., $k$($NO_3$+propane) = $9.49\times10^{-15}$ $cm^3$ $molecule^{-1}$ $s^{-1}$ at 298 K (Atkinson and Arey, 2003). As a result, their combined contribution to total VOC-driven $NO_3$ reactivity is < 5% ($0.04 \times 10^{-3}$ $s^{-1}$), emphasizing that high VOC concentration does not equate to strong $NO_3$ reactivity. When all AVOCs are considered, they dominate $NO_3$ reactivity (~70.4% of total VOC-driven $NO_3$ loss), exceeding the contribution of biogenic VOCs (BVOCs, ~29.6%) (Figure S4).

**Reactive VOCs dominate VOC-driven $NO_3$ loss.** Despite their low concentrations, styrene and isoprene account for ~74% of total VOC-driven $NO_3$ reactivity (Figure S4), due to their high $k_{NO_3}$.

**Styrene:** Average reactivity = $0.34 \times 10^{-3}$ $s^{-1}$ ($k$ = $1.5\times10^{-12}$ $cm^3$ $molecule^{-1}$ $s^{-1}$), contributing ~44% of VOC reactivity. Styrene emissions in Beijing are primarily from vehicle exhaust, with minor contributions from evergreen plant emissions (Li et al., 2014).

**Isoprene:** Average reactivity = $0.25 \times 10^{-3}$ $s^{-1}$, contributing ~30% of VOC reactivity. Isoprene has dual sources: traffic exhaust (anthropogenic) and deciduous/evergreen plant emissions (biogenic), with biogenic sources dominating in winter (Cheng et al., 2018; Yuan et al., 2009).

Notably, biogenic VOCs (BVOCs) other than isoprene (e.g., limonene, α-pinene) were not detected, leading to potential underestimation of BVOC reactivity. For example, the rate constant for limonene (~$1.6\times10^{-11}$ $cm^3$ $molecule^{-1}$ $s^{-1}$) is ~20× higher than isoprene's, so including it could increase the total VOC reactivity.

**γ($N_2O_5$)**—a key parameter describing the efficiency of $N_2O_5$ uptake on aerosol surfaces—was calculated via Eq. (7) (steady-state method) with strict data selection, and the calculation results for $S_a$ are presented in Figure S5. For most of the time, γ($N_2O_5$) ranged from 0.01 to 0.12 (average: 0.032 ± 0.049; Table S2), consistent with observations in urban Beijing (0.01–0.09) (Li et al., 2022; Wang et al., 2017a; Xia et al., 2021; Zhou et al., 2018) but higher than rural sites: Wangdu (Hebei), 0.006–0.034 (Tham et al., 2018); Hong Kong boundary layer, 0.014 ± 0.007 (Brown et al., 2016); Rural Germany, 0.028 ± 0.029 (Phillips et al., 2016). The elevated γ($N_2O_5$) in our study is attributed to urban aerosols' higher water content and reactive composition (e.g., nitrate, sulfate, and organic acids), which enhance $N_2O_5$ hydrolysis efficiency (Bertram et al., 2009; Tang et al., 2014).

### 4.2.2 Temporal Variations in $NO_3$ Reactivity

To characterize how $NO_3$ loss dynamics respond to emission controls and transient environmental events, we analyzed the time series of total $NO_3$ reactivity—the sum of all first-order loss pathways, including reaction

with NO, heterogeneous uptake of $N_2O_5$, oxidation by VOCs, and photolysis (daytime only). This analysis is supported by Figure 5 (time series of total $k_{NO_3}$ and key environmental drivers).

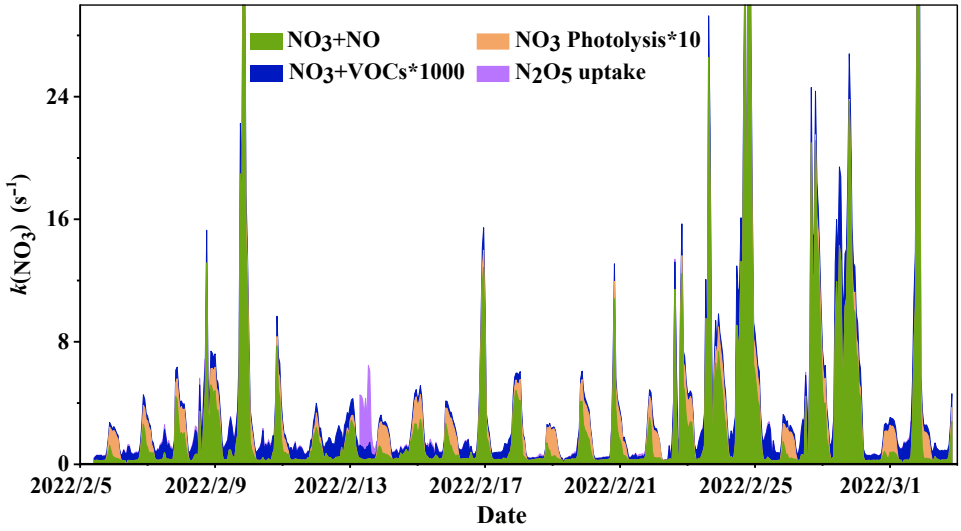


**Figure 5. Time series variation of $k_{NO_3}$ (reactions with NO and VOCs, heterogeneous uptake of $N_2O_5$ and photolysis of $NO_3$).**

**OGP**: Total $k_{NO_3}$ averaged 1.14 $s^{-1}$, with minimal day-to-day variability. A notable exception occurred on 13 February, when a heavy snowfall event (RH = 71%, $PM_{2.5}$ = 61 μg $m^{-3}$) triggered a transient spike in $k_{NO_3}$ to 2.35 $s^{-1}$—nearly double the OGP average. This spike was driven by enhanced $N_2O_5$ heterogeneous uptake (Section 4.1.1), as high RH increased aerosol liquid water content and reactive surface sites.

**POP**: Total $k_{NO_3}$ surged to 3.06 $s^{-1}$ (2.7× higher than OGP), driven by a 3.7× increase in NO reactivity (from 0.81 $s^{-1}$ to 3.00 $s^{-1}$; Table 3). The elevated NO reactivity aligns with post-Olympic NO emission rebound (Section 3.1.2), which intensified $NO_3$ titration (Reaction R4) and crowded out $N_2O_5$ uptake.

Figure 5 also captures the response of $k_{NO_3}$ to transient NO spikes—critical drivers of non-steady-state $NO_3$ loss. For example, on 24 February (POP), a sudden NO burst (24.8 ppbv, Figure S6) caused total $k_{NO_3}$ to jump from 1.3 $s^{-1}$ to 26.5 $s^{-1}$ within 30 minutes, with no corresponding change in RH or $S_a$. This confirms that NO can override the effects of meteorological factors on $k_{NO_3}$ in winter urban environments.

To dissect the drivers of total $k_{NO_3}$ variation, Table 3 presents the contributions of individual reactivity components (NO reaction, $N_2O_5$ uptake, VOC oxidation) for both periods:

**OGP (Table 3)**: Reactivity was dominated by two pathways. (1) NO reaction: Contributed 0.81 $s^{-1}$ (71.1% of total $k_{NO_3}$), reflecting moderate NO emissions under Olympic controls. (2) $N_2O_5$ uptake: Contributed 0.32 $s^{-1}$

(28.1% of total $k_{NO_3}$), with the 13 February snowfall event pushing this contribution to 86% (2.35 $s^{-1}$). VOC oxidation remained negligible at $0.8 \times 10^{-3}$ $s^{-1}$ (< 0.1% of total $k_{NO_3}$), consistent with winter's low VOC emissions and low $NO_3$-VOC reaction rates (Section 4.2.1). For instance, even the styrene contributed only ~44% of total VOC reactivity, which remained orders of magnitude lower than NO-driven reactivity.

**POP (Table 3)**: A dramatic shift in reactivity partitioning occurred. (1) NO reaction: Exploded to 3.00 $s^{-1}$ (98.0% of total $k_{NO_3}$), a 3.7× increase from the OGP. This was driven by post-Olympic NO emissions, which intensified $NO_3$ titration and crowded out other loss pathways. (2) $N_2O_5$ uptake: Plummeted to 0.06 $s^{-1}$ (2.0% of total $k_{NO_3}$), an 81% decrease from the OGP. The decline stemmed from lower POP RH (19% vs. 27% in OGP), which reduced aerosol liquid water content and suppressed $N_2O_5$ hydrolysis (Reaction R6). This RH-dependent hydrolysis inhibition is further validated by Figure S7 (auxiliary material): the figure presents the correlation between $N_2O_5$ hydrolysis rate and RH during the POP, showing a strong positive linear relationship ($R^2$= 0.81). The reduced hydrolysis efficiency directly limited $N_2O_5$'s role as an indirect $NO_3$ sink, contributing to its diminished share of $NO_3$ loss in the POP. VOC oxidation increased slightly to $1.4 \times 10^{-3}$ $s^{-1}$ (< 0.1% of total $k_{NO_3}$), reflecting a modest rebound in anthropogenic VOC emissions (Table 2: total VOCs = 19.68 ppbv vs. 16.02 ppbv in OGP) but remained functionally irrelevant to $NO_3$ loss.

**Table 3 Statistics of $k_{NO_3}$ across various pathways and time periods**

| $k_{NO_3}$ ($s^{-1}$) | OGP | POP |
|---|---|---|
| $NO_3$+NO | 0.81 | 3.00 |
| $NO_3$+VOCs | $0.8 \times 10^{-3}$ | $1.4 \times 10^{-3}$ |
| $N_2O_5$ uptake | 0.32 | 0.06 |
| Total | 1.14 | 3.06 |

The combined analysis of Figure 5 (total trend) and Table 3 reveals two critical findings:

**Emission controls rewire reactivity partitioning**: Olympic $NO_x$ reductions reduced NO's dominance as a $NO_3$ sink, allowing $N_2O_5$ uptake to emerge as a significant secondary pathway. Relaxing controls reversed this shift, reestablishing NO as the near-exclusive $NO_3$ loss mechanism.

**Extreme events disrupt baseline reactivity**: High-RH events (e.g., snowfall) and NO spikes can temporarily alter reactivity partitioning, but their effects are transient—baseline dynamics remain governed by long-term emission conditions.

### 4.2.3 $NO_3$ loss budget

Figure 6 illustrates the diurnal variation and relative contributions of $NO_3$ loss pathways, with distinct differences between the OGP and POP that reflect the impact of Olympic emission controls.

**OGP: Balanced NO and $N_2O_5$ uptake pathways.** NO dominated $NO_3$ loss (79.0%), but $N_2O_5$ uptake emerged as a significant secondary pathway (20.8%), with VOC oxidation contributing < 0.2%. The $N_2O_5$ uptake pathway peaked at 19:00 LST (0.37 ppbv $h^{-1}$), coinciding with high [$N_2O_5$] (149.9 pptv). This contribution is comparable to winter observations in urban Beijing (Li et al., 2022).

**POP: NO dominates $NO_3$ loss.** NO's contribution to $NO_3$ loss rose to 89.4%, with a peak loss rate of 2.04 ppbv $h^{-1}$ at 22:00 LST—driven by post-Olympic NO emissions that increased significantly (Table 2). In contrast, $N_2O_5$ uptake declined to 10.6%, as lower RH reduced $\gamma(N_2O_5)$ and $S_a$ reactivity. Notably, the POP's $NO_3$ loss rate (1.61 ppbv $h^{-1}$) was 30% higher than the OGP's (1.14 ppbv $h^{-1}$), confirming that relaxed emissions accelerated nocturnal $NO_3$ removal.

Compared to summer studies (Lin et al., 2022), winter's low VOC reactivity and high NO emissions make NO the unambiguous primary $NO_3$ sink in urban Beijing. This seasonal contrast underscores the need for season-specific air quality management strategies—prioritizing $NO_x$ reduction in winter and VOC reduction in summer.

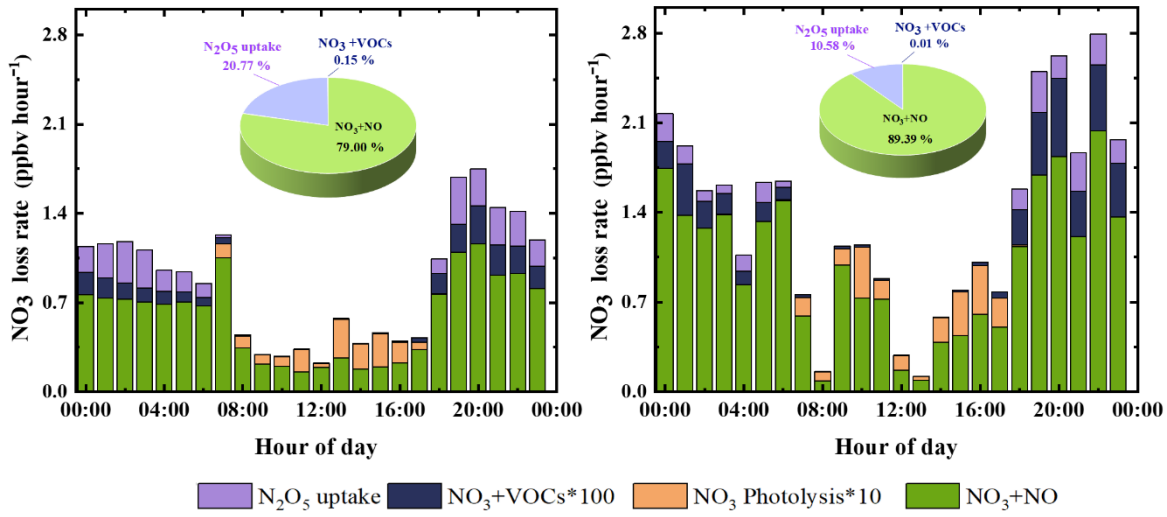


**Figure 6. Mean daily variation and reactivity share of different loss pathways.**

### 4.3 Linkage to Olympic Emission Controls and Precursor Dynamics

The 2022 Beijing Winter Olympics provided a unique "natural experiment" to quantify how short-term, large-scale emission controls modulate nocturnal $NO_3$-$N_2O_5$ chemistry. Below, we dissect the impacts of these controls on precursor concentrations and loss pathway hierarchies, and explore the interacting roles of $NO_2$ and $O_3$ in shaping $NO_3$-$N_2O_5$ dynamics.

#### 4.3.1 Impact of Emission Controls on $NO_3$-$N_2O_5$ Chemistry

The Olympic emission control measures—including traffic restrictions (e.g., odd-even license plate policy), industrial shutdowns, and reduced coal combustion—induced significant changes in precursor concentrations

and $NO_3$-$N_2O_5$ behavior.

**Precursor modulation**: OGP emissions of $NO_x$ and VOCs were substantially lower than the POP. Nocturnal NO decreased by 79% (1.0 vs. 4.8 ppbv), and $NO_2$ by 30% (14.5 vs. 20.7 ppbv). Nocturnal total VOCs decreased by 18% (16.02 vs. 19.68 ppbv), with reactive AVOCs (styrene) declining by 40%.

Lower NO emissions weakened its role as a "$NO_3$ scavenger," allowing more $NO_3$ to partition into $N_2O_5$ via Reaction R2. This explains why the OGP's nocturnal [$N_2O_5$] (137.6 pptv) was 41% higher than the POP's (97.8 pptv), despite similar $NO_3$ production rates ($P(NO_3)$ = 0.5 ppbv $h^{-1}$ for both periods).

**Loss pathway shift**: Reduced NO emissions elevated the relative importance of $N_2O_5$ uptake in $NO_3$ loss—its contribution increased from 10.6% (POP) to 20.8% (OGP). This shift demonstrates that emission controls can "rewire" nocturnal loss hierarchies, making heterogeneous processes more significant as primary pollutant emissions decline. This finding extends previous studies (Xia et al., 2020; Zhou et al., 2018a) which focused on $ClNO_2$ formation but did not quantify $N_2O_5$'s role under low-NO conditions.

### 4.3.2 Precursor ($NO_2$, $O_3$) Influences on $NO_3$-$N_2O_5$ Dynamics

$NO_2$ and $O_3$, the primary precursors of $NO_3$ via Reaction R1, exert dual and interactive controls on $NO_3$-$N_2O_5$ chemistry that depend on emission conditions.

**$NO_2$: Equilibrium driver and precursor tradeoff.** $NO_2$ plays two conflicting roles: it is both a precursor for $NO_3$ (via R1) and a partner in the $NO_3$-$N_2O_5$ equilibrium (via R2). During the OGP, higher nocturnal $NO_2$ (14.5 ppbv) shifted the equilibrium toward $N_2O_5$, as low NO prevented rapid $NO_3$ loss. This created a "$N_2O_5$ surplus," with [$N_2O_5$] exceeding the POP's by 41%. In contrast, the POP's higher $NO_2$ (20.7 ppbv) paired with elevated NO (4.8 ppbv) created a "dual sink" effect: more $NO_3$ was produced via R1, but immediately titrated by NO via R4—limiting $N_2O_5$ accumulation. This tradeoff highlights $NO_2$'s context-dependent role in $NO_3$-$N_2O_5$ dynamics.

**$O_3$: Production regulator and persistence enhancer.** OGP's higher nocturnal $O_3$ (27.4 vs. 19.8 ppbv in the POP) initially boosted $NO_3$ production ($P(NO_3)$ = 0.5 ppbv $h^{-1}$), but lower NO prevented rapid $NO_3$ loss. This "$NO_3$ surplus" prolonged $N_2O_5$ lifetime: the OGP's nocturnal $\tau_{N_2O_5}$ (17.0 minutes) was 46% longer than the POP's (11.6 minutes). This indirect effect of $O_3$—enhancing $N_2O_5$ persistence by supporting $NO_3$ production without accelerating loss—has not been fully quantified in previous winter studies, emphasizing the need to consider $O_3$ alongside $NO_x$ in nocturnal chemistry models.

## 4.4 Broader Atmospheric Implications

Our findings advance understanding of winter urban nocturnal chemistry and provide critical insights for air

quality management in polluted regions like Beijing. Three key implications emerge:

**Emission control efficacy and regional nitrate transport.** Olympic controls demonstrated that reducing $NO_x$ (not just VOCs) can enhance $N_2O_5$ accumulation—potentially extending the lifetime of reactive nitrogen and increasing regional nitrate transport. $N_2O_5$ is a stable reservoir species that can be transported long distances before hydrolyzing to form nitrate aerosols; thus, increased $N_2O_5$ under $NO_x$ reduction may shift winter nitrate pollution from local to regional scales. This suggests that future $NO_x$ mitigation strategies should consider regional coordination to address long-range transport of reactive nitrogen.

**Model parameterization improvements.** Our results provide two critical constraints for air quality models, which often underestimate winter $N_2O_5$ chemistry.

**$S_a$ threshold**: $S_a$ exerts significant control over $\tau_{N_2O_5}$ only when $S_a > 500$ μm² cm$^{-3}$; below this threshold, organic coatings and NO dominate.

**$\gamma(N_2O_5)$ range**: The average $\gamma(N_2O_5)$ of 0.032 ± 0.049 (with values up to 0.22 under high RH) is higher than the constant $\gamma(N_2O_5) = 0.02$ (Chang et al., 2011) often used in models. Incorporating these season-specific parameters will improve predictions of winter nitrate formation.

**Winter mitigation priority: $NO_x$ over VOCs.** Despite their high reactivity, VOCs contribute < 0.5% of $NO_3$ loss in winter urban Beijing—far less than NO (79.0–89.4%). This confirms that $NO_x$ (not VOCs) should be prioritized for mitigating winter nocturnal nitrogen pollution. For example, further reducing traffic-related NO emissions (a major source in urban Beijing) would not only lower direct NO pollution but also enhance $N_2O_5$ uptake—a pathway that converts reactive nitrogen to nitrate, which is less toxic and more easily removed via wet deposition.

## 5 Summary and conclusions

This study conducted continuous field observations of $N_2O_5$, $NO_3$, and their precursor species (NO, $NO_2$, $O_3$, VOCs) in urban Beijing from 5 February to 3 March 2022, covering the 2022 Beijing Winter Olympics (BWO). By analyzing pollutant variations, quantifying the contributions of $NO_3/N_2O_5$ loss pathways, and linking observations to BWO emission control measures, we clarified the response of winter nocturnal reactive nitrogen chemistry to short-term anthropogenic emission reductions.

During the observation period, $P(NO_3)$ averaged 0.5 ± 0.4 ppbv h$^{-1}$, with $N_2O_5$ mixing ratios peaking at 875 pptv (1-minute resolution) and derived $NO_3$ concentrations reaching a maximum of 4.6 pptv; $\tau_{N_2O_5}$ averaged 11.9 ± 11.8 minutes, longer than summer values in Beijing due to slower winter $N_2O_5$ loss driven by low temperatures and reduced heterogeneous reactivity. BWO emission controls significantly modulated precursor concentrations: nocturnal NO (1.0 ± 1.2 ppbv) and total VOCs (16.02 ± 7.74 ppbv) in the OGP were 79% and

18% lower than in the POP, respectively, while nocturnal $O_3$ was 38% higher in the OGP (27.4 ± 10.3 ppbv vs. 19.8 ± 12.1 ppbv in the POP) as reduced NO minimized $O_3$ titration—these changes directly led to 41% higher nocturnal $N_2O_5$ concentrations in the OGP (137.6 ± 112.7 pptv vs. 97.8 ± 90.3 pptv in the POP).

RH and $S_a$ exerted context-dependent control over $\tau_{N_2O_5}$: at RH < 35%, $\tau_{N_2O_5}$ increased with RH as slight humidity rises softened hydrophobic organic aerosol coatings (derived from traffic VOC oxidation) and reduced $N_2O_5$ heterogeneous uptake; at RH > 35%, $\tau_{N_2O_5}$ decreased with RH due to hygroscopic aerosol growth and enhanced $N_2O_5$ hydrolysis, approaching zero during snowfall events (RH > 85%). For $S_a$, a threshold of ~500 $\mu m^2\ cm^{-3}$ was identified—below this value, organic coatings and NO dominated $\tau_{N_2O_5}$; above it, $S_a$ became the primary regulator, with $\tau_{N_2O_5}$ decreasing as $S_a$ increased.

NO was the dominant $NO_3$ sink in both periods, though its contribution varied with emission controls: it accounted for 79.0% of $NO_3$ loss in the OGP, with $N_2O_5$ heterogeneous uptake (20.8%) as a significant secondary pathway, while its contribution rose to 89.2% in the POP (driven by 3.8× higher NO emissions) and $N_2O_5$ uptake declined to 10.6% (due to lower RH reducing aerosol reactivity). The $N_2O_5$ heterogeneous uptake coefficient ($\gamma(N_2O_5)$) averaged 0.032 ± 0.049 in the OGP, higher than rural sites due to urban aerosols' higher water content and reactive components (e.g., nitrate, sulfate). Despite the high reactivity of species like styrene and isoprene, VOC oxidation contributed < 0.2% to $NO_3$ loss in both periods, confirming its negligible role in winter $NO_3$ dynamics in urban Beijing.

These findings hold key implications for air quality management: BWO $NO_x$ reductions enhanced $N_2O_5$ accumulation, potentially extending reactive nitrogen lifetime and shifting winter nitrate pollution from local to regional scales—highlighting the need for regional coordination in $NO_x$ mitigation; the identified $S_a$ threshold (500 $\mu m^2\ cm^{-3}$) and $\gamma(N_2O_5)$ range (0.01–0.12) provide critical constraints for air quality models, which often rely on oversimplified $\tau_{N_2O_5}$ and $\gamma(N_2O_5)$ parameters; and given NO's dominance in $NO_3$ loss and $N_2O_5$ dynamics, $NO_x$ (not VOCs) should be prioritized for winter nocturnal nitrogen pollution control in Beijing—reducing traffic-related NO emissions would simultaneously lower direct pollution and enhance $N_2O_5$ uptake, promoting nitrate removal via wet deposition.

**Data availability.** Data are available at https://doi.org/10.5281/zenodo.15381990 (T. Zhang et al., 2025).

**Author Contributions.** TZ, WL and CY designed the research. WL and CY organized this field campaign. TZ, PZ, YC, TL and LZ carried out the field measurements and provided the field measurement dataset. TZ performed data analysis, interpreted the data and wrote the manuscript with revision mainly from WL. All authors have given approval to the final version of the manuscript.

**Competing interests.** The contact author has declared that none of the authors has any competing interests.

**Disclaimer.** Publisher's note: Copernicus Publications remains neutral with regard to jurisdictional claims in published maps and institutional affiliations.

**Acknowledgment.** The authors would like to thank the field campaign team for the data that they contributed during the 2022 Beijing Winter Olympics.

**Financial support.** This study was financially supported by the National Natural Science Foundation of China (42405083), the National Key Research and Development Program (2024YFC3711902).

## References

Anttila, T., Kiendler-Scharr, A., Tillmann, R., and Mentel, T. F.: On the Reactive Uptake of Gaseous Compounds by Organic-Coated Aqueous Aerosols: Theoretical Analysis and Application to the Heterogeneous Hydrolysis of $N_2O_5$, J. Phys. Chem. A, 110, 10435–10443, https://doi.org/10.1021/jp062403c, 2006.

Atkinson, R. and Arey, J.: Atmospheric Degradation of Volatile Organic Compounds, Chem. Rev., 103, 4605–4638, https://doi.org/10.1021/cr0206420, 2003.

Atkinson, R., Baulch, D. L., Cox, R. A., Crowley, J. N., Hampson, R. F., Hynes, R. G., Jenkin, M. E., Rossi, M. J., and Troe, J.: Evaluated kinetic and photochemical data for atmospheric chemistry: Volume I - gas phase reactions of $O_x$, $HO_2$, $NO_x$ and $SO_x$ species, Atmos. Chem. Phys., 4, 1461–1738, https://doi.org/10.5194/acp-4-1461-2004, 2004.

Bertram, T. H., Thornton, J. A., Riedel, T. P., Middlebrook, A. M., Bahreini, R., Bates, T. S., Quinn, P. K., and Coffman, D. J.: Direct observations of $N_2O_5$ reactivity on ambient aerosol particles, Geophys. Res. Lett., 36, L19803, https://doi.org/10.1029/2009GL040248, 2009.

Bohn, B., Corlett, G. K., Gillmann, M., Sanghavi, S., Stange, G., Tensing, E., Vrekoussis, M., Bloss, W. J., Clapp, L. J., Kortner, M., Dorn, H.-P., Monks, P. S., Platt, U., Plass-Dülmer, C., Mihalopoulos, N., Heard, D. E., Clemitshaw, K. C., Meixner, F. X., Prevot, A. S. H., and Schmitt, R.: Photolysis frequency measurement techniques: results of a comparison within the ACCENT project, Atmos. Chem. Phys., 8, 5373–5391, https://doi.org/10.5194/acp-8-5373-2008, 2008.

Brown, S. S. and Stutz, J.: Nighttime radical observations and chemistry, Chem. Soc. Rev., 41, 6405, https://doi.org/10.1039/c2cs35181a, 2012.

Brown, S. S., Dubé, W. P., Peischl, J., Ryerson, T. B., Atlas, E., Warneke, C., de Gouw, J. A., te Lintel Hekkert, S., Brock, C. A., Flocke, F., Trainer, M., Parrish, D. D., Feshenfeld, F. C., and Ravishankara, A. R.: Budgets for nocturnal VOC oxidation by nitrate radicals aloft during the 2006 Texas Air Quality Study, J. Geophys. Res., 116, 1–15, https://doi.org/10.1029/2011JD016544, 2011.

Brown, S. S., Dubé, W. P., Tham, Y. J., Zha, Q., Xue, L., Poon, S., Wang, Z., Blake, D. R., Tsui, W., Parrish, D. D., and Wang, T.: Nighttime chemistry at a high altitude site above Hong Kong, J. Geophys. Res. Atmos., 121, 2457–2475, https://doi.org/10.1002/2015JD024566, 2016.

Brown, S. S., An, H., Lee, M., Park, J.-H., Lee, S.-D., Fibiger, D. L., McDuffie, E. E., Dubé, W. P., Wagner, N.

L., and Min, K.-E.: Cavity enhanced spectroscopy for measurement of nitrogen oxides in the Anthropocene: results from the Seoul tower during MAPS 2015, Faraday Discuss., 200, 529–557, https://doi.org/10.1039/C7FD00001D, 2017.

Chang, W. L., Bhave, P. V., Brown, S. S., Riemer, N., Stutz, J., and Dabdub, D.: Heterogeneous Atmospheric Chemistry, Ambient Measurements, and Model Calculations of $N_2O_5$: A Review, Aerosol Sci. Technol., 45, 665–695, https://doi.org/10.1080/02786826.2010.551672, 2011.

Cheng, X., Li, H., Zhang, Y., and Li, Y.: Atmospheric isoprene and monoterpenes in a typical urban area of Beijing: Pollution characterization, chemical reactivity and source identification, J. Environ. Sci., 71, 150–167, https://doi.org/10.1016/j.jes.2017.12.017, 2018.

Crutzen, P. J.: The Role of NO and $NO_2$ in the Chemistry of the Troposphere and Stratosphere, Annu. Rev. Earth Planet. Sci., 7, 443–472, https://doi.org/10.1146/annurev.ea.07.050179.002303, 1979.

Folkers, M., Mentel, Th. F., and Wahner, A.: Influence of an organic coating on the reactivity of aqueous aerosols probed by the heterogeneous hydrolysis of $N_2O_5$, Geophys. Res. Lett., 30, 2003GL017168, https://doi.org/10.1029/2003GL017168, 2003.

Fry, J. L. and Sackinger, K.: Model investigation of $NO_3$ secondary organic aerosol (SOA) source and heterogeneous organic aerosol (OA) sink in the western United States, Atmos. Chem. Phys., 12, 8797–8811, https://doi.org/10.5194/acp-12-8797-2012, 2012.

Hoyle, C. R., Berntsen, T., Myhre, G., and Isaksen, I. S. A.: Secondary organic aerosol in the global aerosol - chemical transport model Oslo CTM2, Atmos. Chem. Phys., 7, 5675–5694, https://doi.org/10.5194/acp-7-5675-2007, 2007.

Hu, H., Wang, H., Lu, K., Wang, J., Zheng, Z., Xu, X., Zhai, T., Chen, X., Lu, X., Fu, W., Li, X., Zeng, L., Hu, M., Zhang, Y., and Fan, S.: Variation and trend of nitrate radical reactivity towards volatile organic compounds in Beijing, China, Atmos. Chem. Phys., 23, 8211–8223, https://doi.org/10.5194/acp-23-8211-2023, 2023.

Huang Z., Hu W., Jin R., Hou S., LI P., Bi K., He C., Wang Y., Duan P., Liu D., Wu L., Deng J., Sun Y., and Fu P.: Chemical composition and sources of fine particles in Beijing around the Winter Olympics, China Environ. Sci., 44, 5344–5356, https://doi.org/10.19674/j.cnki.issn1000-6923.20240604.002, 2024.

Li, H., Zheng, B., Lei, Y., Hauglustaine, D., Chen, C., Lin, X., Zhang, Y., Zhang, Q., and He, K.: Trends and drivers of anthropogenic $NO_x$ emissions in China since 2020, Environ. Sci. Ecotechnol., 21, 100425, https://doi.org/10.1016/j.ese.2024.100425, 2024.

Li, L., Li, H., and Zhang, X.: Pollution characteristics and health risk assessment of benzene homologues in ambient air in the northeastern urban area of Beijing, China, J. Environ. Sci., 26, 214–223, https://doi.org/10.1016/S1001-0742(13)60400-3, 2014.

Li, Z., Xie, P., Hu, R., Wang, D., Jin, H., Chen, H., Lin, C., and Liu, W.: Observations of $N_2O_5$ and $NO_3$ at a suburban environment in Yangtze river delta in China: Estimating heterogeneous $N_2O_5$ uptake coefficients, J. Environ. Sci., 95, 248–255, https://doi.org/10.1016/j.jes.2020.04.041, 2020.

Li, Z., Wang, D., Xie, P., Hu, R., Chen, H., and Lin, C.: Nighttime $N_2O_5$ chemistry in an urban site of Beijing

in winter based on the measurements by cavity ring-down spectroscopy, Air Qual. Atmos. Hlth., 15, 867–876, https://doi.org/10.1007/s11869-021-01125-4, 2022.

Lin, C., Hu, R., Xie, P., Lou, S., Zhang, G., Tong, J., Liu, J., and Liu, W.: Nocturnal atmospheric chemistry of $NO_3$ and $N_2O_5$ over Changzhou in the Yangtze River Delta in China, J. Environ. Sci., 114, 376–390, https://doi.org/10.1016/j.jes.2021.09.016, 2022.

Lu, X., Qin, M., Xie, P., Duan, J., Fang, W., and Liu, W.: Observation of ambient $NO_3$ radicals by LP-DOAS at a rural site in North China Plain, Sci. Total Environ., 804, 149680, https://doi.org/10.1016/j.scitotenv.2021.149680, 2022.

McNeill, V. F., Patterson, J., Wolfe, G. M., and Thornton, J. A.: The effect of varying levels of surfactant on the reactive uptake of $N_2O_5$ to aqueous aerosol, Atmos. Chem. Phys., 6, 1635–1644, https://doi.org/10.5194/acp-6-1635-2006, 2006.

Ng, N. L., Brown, S. S., Archibald, A. T., Atlas, E., Cohen, R. C., Crowley, J. N., Day, D. A., Donahue, N. M., Fry, J. L., Fuchs, H., Griffin, R. J., Guzman, M. I., Herrmann, H., Hodzic, A., Iinuma, Y., Jimenez, J. L., Kiendler-Scharr, A., Lee, B. H., Luecken, D. J., Mao, J., McLaren, R., Mutzel, A., Osthoff, H. D., Ouyang, B., Picquet-Varrault, B., Platt, U., Pye, H. O. T., Rudich, Y., Schwantes, R. H., Shiraiwa, M., Stutz, J., Thornton, J. A., Tilgner, A., Williams, B. J., and Zaveri, R. A.: Nitrate radicals and biogenic volatile organic compounds: oxidation, mechanisms, and organic aerosol, Atmos. Chem. Phys., 17, 2103–2162, https://doi.org/10.5194/acp-17-2103-2017, 2017.

Osthoff, H. D., Sommariva, R., Baynard, T., Pettersson, A., Williams, E. J., Lerner, B. M., Roberts, J. M., Stark, H., Goldan, P. D., Kuster, W. C., Bates, T. S., Coffman, D., Ravishankara, A. R., and Brown, S. S.: Observation of daytime$N_2O_5$ in the marine boundary layer during New England Air Quality Study–Intercontinental Transport and Chemical Transformation 2004, J. Geophys. Res. Atmospheres, 111, https://doi.org/10.1029/2006JD007593, 2006.

Phillips, G. J., Thieser, J., Tang, M. J., Sobanski, N., Schuster, G., Fachinger, J., Drewnick, F., Borrmann, S., Bingemer, H., Lelieveld, J., and Crowley, J. N.: Estimating $N_2O_5$ uptake coefficients using ambient measurements of $NO_3$,$N_2O_5$, $ClNO_2$ and particle-phase nitrate, Atmos. Chem. Phys., 1–9, https://doi.org/10.5194/acp-2016-693, 2016.

Pye, H. O. T., Chan, A. W. H., Barkley, M. P., and Seinfeld, J. H.: Global modeling of organic aerosol: the importance of reactive nitrogen ($NO_x$ and $NO_3$), Atmos. Chem. Phys., 10, 11261–11276, https://doi.org/10.5194/acp-10-11261-2010, 2010.

Tang, M. J., Schuster, G., and Crowley, J. N.: Heterogeneous reaction of $N_2O_5$ with illite and Arizona test dust particles, Atmos. Chem. Phys., 14, 245–254, https://doi.org/10.5194/acp-14-245-2014, 2014.

Tham, Y. J., Wang, Z., Li, Q., Yun, H., Wang, W., Wang, X., Xue, L., Lu, K., Ma, N., Bohn, B., Li, X., Kecorius, S., Größ, J., Shao, M., Wiedensohler, A., Zhang, Y., and Wang, T.: Significant concentrations of nitryl chloride sustained in the morning: investigations of the causes and impacts on ozone production in a polluted region of northern China, Atmos. Chem. Phys., 16, 14959–14977, https://doi.org/10.5194/acp-16-14959-2016, 2016.

Tham, Y. J., Wang, Z., Li, Q., Wang, W., Wang, X., Lu, K., Ma, N., Yan, C., Kecorius, S., Wiedensohler, A., Zhang, Y., and Wang, T.: Heterogeneous $N_2O_5$ uptake coefficient and production yield of $ClNO_2$ in polluted northern China: roles of aerosol water content and chemical composition, Atmos. Chem. Phys., 18, 13155–13171, https://doi.org/10.5194/acp-18-13155-2018, 2018.

Wang, D., Xie, P., Hu, R., Li, Z., Chen, H., and Jin, H.: Reactivity and Loss Mechanisms of $NO_3$ and $N_2O_5$ at a Rural Site on the North China Plain, Atmosphere, 13, 1268, https://doi.org/10.3390/atmos13081268, 2022.

Wang, H., Lu, K., Chen, X., Zhu, Q., Chen, Q., Guo, S., Jiang, M., Li, X., Shang, D., Tan, Z., Wu, Y., Wu, Z., Zou, Q., Zheng, Y., Zeng, L., Zhu, T., Hu, M., and Zhang, Y.: High $N_2O_5$ Concentrations Observed in Urban Beijing: Implications of a Large Nitrate Formation Pathway, Environ. Sci. Technol. Lett., 4, 416–420, https://doi.org/10.1021/acs.estlett.7b00341, 2017a.

Wang, H., Lu, K., Guo, S., Wu, Z., Shang, D., Tan, Z., Wang, Y., Le Breton, M., Lou, S., Tang, M., Wu, Y., Zhu, W., Zheng, J., Zeng, L., Hallquist, M., Hu, M., and Zhang, Y.: Efficient $N_2O_5$ uptake and $NO_3$ oxidation in the outflow of urban Beijing, Atmos. Chem. Phys., 18, 9705–9721, https://doi.org/10.5194/acp-18-9705-2018, 2018.

Wang, H., Chen, X., Lu, K., Hu, R., Li, Z., Wang, H., Ma, X., Yang, X., Chen, S., Dong, H., Liu, Y., Fang, X., Zeng, L., Hu, M., and Zhang, Y.: $NO_3$ and $N_2O_5$ chemistry at a suburban site during the EXPLORE-YRD campaign in 2018, Atmos. Environ., 224, 117180, https://doi.org/10.1016/j.atmosenv.2019.117180, 2020.

Wang, H., Lu, K., Chen, S., Li, X., Zeng, L., Hu, M., and Zhang, Y.: Characterizing nitrate radical budget trends in Beijing during 2013–2019, Sci. Total Environ., 795, 148869, https://doi.org/10.1016/j.scitotenv.2021.148869, 2021.

Wang, H., Wang, H., Lu, X., Lu, K., Zhang, L., Tham, Y. J., Shi, Z., Aikin, K., Fan, S., Brown, S. S., and Zhang, Y.: Increased night-time oxidation over China despite widespread decrease across the globe, Nat. Geosci., 16, 217–223, https://doi.org/10.1038/s41561-022-01122-x, 2023a.

Wang, J., Wang, H., Tham, Y. J., Ming, L., Zheng, Z., Fang, G., Sun, C., Ling, Z., Zhao, J., and Fan, S.: Measurement report: Atmospheric nitrate radical chemistry in the South China Sea influenced by the urban outflow of the Pearl River Delta, Atmos. Chem. Phys., 24, 977–992, https://doi.org/10.5194/acp-24-977-2024, 2024.

Wang, M., Zeng, L., Lu, S., Shao, M., Liu, X., Yu, X., Chen, W., Yuan, B., Zhang, Q., Hu, M., and Zhang, Z.: Development and validation of a cryogen-free automatic gas chromatograph system (GC-MS/FID) for online measurements of volatile organic compounds, Anal. Methods, 6, 9424–9434, https://doi.org/10.1039/C4AY01855A, 2014.

Wang, S., Shi, C., Zhou, B., Zhao, H., Wang, Z., Yang, S., and Chen, L.: Observation of $NO_3$ radicals over Shanghai, China, Atmos. Environ., 70, 401–409, https://doi.org/10.1016/j.atmosenv.2013.01.022, 2013.

Wang, X., Wang, H., Xue, L., Wang, T., Wang, L., Gu, R., Wang, W., Tham, Y. J., Wang, Z., Yang, L., Chen, J., and Wang, W.: Observations of $N_2O_5$ and $ClNO_2$ at a polluted urban surface site in North China: High $N_2O_5$ uptake coefficients and low $ClNO_2$ product yields, Atmos. Environ., 156, 125–134, https://doi.org/10.1016/j.atmosenv.2017.02.035, 2017b.

744 Wang, Y., Xi, S., Zhao, F., Huey, L. G., and Zhu, T.: Decreasing Production and Potential Urban Explosion of
745 Nighttime Nitrate Radicals amid Emission Reduction Efforts, Environ. Sci. Technol., 57, 21306–21312,
746 https://doi.org/10.1021/acs.est.3c09259, 2023b.
747 Wang, Z., Wang, W., Tham, Y. J., Li, Q., Wang, H., Wen, L., Wang, X., and Wang, T.: Fast heterogeneous $N_2O_5$
748 uptake and $ClNO_2$ production in power plant and industrial plumes observed in the nocturnal residual layer
749 over the North China Plain, Atmos. Chem. Phys., 17, 12361–12378, https://doi.org/10.5194/acp-17-12361-
750 2017, 2017c.
751 Wayne, R. P., Barnes, I., Biggs, P., Burrows, J. P., Canosa-Mas, C. E., Hjorth, J., Le Bras, G., Moortgat, G. K.,
752 Perner, D., Poulet, G., Restelli, G., and Sidebottom, H.: The nitrate radical: Physics, chemistry, and the
753 atmosphere, Atmos. Environ. Part Gen. Top., 25, 1–203, https://doi.org/10.1016/0960-1686(91)90192-A,
754 1991.
755 Xia, M., Peng, X., Wang, W., Yu, C., Sun, P., Li, Y., Liu, Y., Xu, Z., Wang, Z., Xu, Z., Nie, W., Ding, A., and
756 Wang, T.: Significant production of $ClNO_2$ and possible source of $Cl_2$ from $N_2O_5$ uptake at a suburban site
757 in eastern China, Atmos. Chem. Phys., 20, 6147–6158, https://doi.org/10.5194/acp-20-6147-2020, 2020.
758 Xia, M., Peng, X., Wang, W., Yu, C., Wang, Z., Tham, Y. J., Chen, J., Chen, H., Mu, Y., Zhang, C., Liu, P., Xue,
759 L., Wang, X., Gao, J., Li, H., and Wang, T.: Winter $ClNO_2$ formation in the region of fresh anthropogenic
760 emissions: seasonal variability and insights into daytime peaks in northern China, Atmos. Chem. Phys., 21,
761 15985–16000, https://doi.org/10.5194/acp-21-15985-2021, 2021.
762 Yan, C., Yee Jun, T., Nie, W., Xia, M., Wang, H., Guo, Y., Ma, W., Zhan, J., Li, Y., Deng, C., Li, Y., Zheng, F.,
763 Chen, X., Li, Q., Zhang, G., Mahajan, A., Cuevas, C. A., Huang, D., and Kulmala, M.: Increasing
764 contribution of nighttime nitrogen chemistry to wintertime haze formation in Beijing observed during
765 COVID-19 lockdowns, Nat. Geosci., 16, https://doi.org/10.1038/s41561-023-01285-1, 2023.
766 Yao Y., Wang S., Wei N., Ye C., Zhang C., Gu X., Zhao W., and Zhang W.: Analysis of surface ozone sources
767 in Beijing during the 2022 Beijing Winter Olympic Games based on total peroxyl radical measurement,
768 Acta Sci. Circumst., 43, 290–297, https://doi.org/10.13671/j.hjkxxb.2023.0070, 2023.
769 Yu, C., Wang, Z., Xia, M., Fu, X., Wang, W., Tham, Y. J., Chen, T., Zheng, P., Li, H., Shan, Y., Wang, X., Xue,
770 L., Zhou, Y., Yue, D., Ou, Y., Gao, J., Lu, K., Brown, S. S., Zhang, Y., and Wang, T.: Heterogeneous $N_2O_5$
771 reactions on atmospheric aerosols at four Chinese sites: improving model representation of uptake
772 parameters, Atmos. Chem. Phys., 20, 4367–4378, https://doi.org/10.5194/acp-20-4367-2020, 2020.
773 Yuan, Z., Lau, A. K. H., Shao, M., Louie, P. K. K., Liu, S. C., and Zhu, T.: Source analysis of volatile organic
774 compounds by positive matrix factorization in urban and rural environments in Beijing, J. Geophys. Res.
775 Atmospheres, 114, https://doi.org/10.1029/2008JD011190, 2009.
776 Yun, H., Wang, W., Wang, T., Xia, M., Yu, C., Wang, Z., Poon, S. C. N., Yue, D., and Zhou, Y.: Nitrate formation
777 from heterogeneous uptake of dinitrogen pentoxide during a severe winter haze in southern China, Atmos.
778 Chem. Phys., 18, 17515–17527, https://doi.org/10.5194/acp-18-17515-2018, 2018.
779 Zhang, H., Wang, S., and Hao, J.: Air pollution and control action in Beijing, J. Clean. Prod., 112, 1519–1527,
780 https://doi.org/10.1016/j.jclepro.2015.04.092, 2016.

Zhang T., Zuo P., Ma J., Ye C., Lin W., and Zhu T.: Characterization and Application of an Online Measurement System for $NO_3$ and $N_2O_5$ Based on Cavity Ring-Down Spectroscopy, Acta Sci. Nat. Univ. Pekin., 60, 563–574, https://doi.org/10.13209/j.0479-8023.2024.030, 2024.

Zhang, T., Ma, J., Liu, T., Lin, W., Zuo, P., and Ye, C.: A dynamic generation system for $NO_3$ and $N_2O_5$ standard gases, Environ. Chem., 45, 1–7, https://doi.org/10.7524/j.issn.0254-6108.2024091302, 2026.

Zhang, T., Zuo, P., Chen, Y., Liu, T., Zeng, L., Lin, W., and Ye, C.: Measurement report: Variations and environmental impacts of atmospheric $N_2O_5$ concentrations in urban Beijing during the 2022 Winter Olympics, Zenodo [data set], https://doi.org/10.5281/zenodo.15381990, 2025.

Zhou, J., Zhao, W., Zhang, Y., Fang, B., Cheng, F., Xu, X., Ni, S., Zhang, W., Ye, C., Chen, W., and Venables, D. S.: Amplitude-Modulated Cavity-Enhanced Absorption Spectroscopy with Phase-Sensitive Detection: A New Approach Applied to the Fast and Sensitive Detection of $NO_2$, Anal. Chem., 94, 3368–3375, https://doi.org/10.1021/acs.analchem.1c05484, 2022.

Zhou, W., Zhao, J., Ouyang, B., Mehra, A., Xu, W., Wang, Y., Bannan, T. J., Worrall, S. D., Priestley, M., Bacak, A., Chen, Q., Xie, C., Wang, Q., Wang, J., Du, W., Zhang, Y., Ge, X., Ye, P., Lee, J. D., Fu, P., Wang, Z., Worsnop, D., Jones, R., Percival, C. J., Coe, H., and Sun, Y.: Production of $N_2O_5$ and $ClNO_2$ in summer in urban Beijing, China, Atmos. Chem. Phys., 18, 11581–11597, https://doi.org/10.5194/acp-18-11581-2018, 2018.

Zhu, T., Tang, M., Gao, M., Bi, X., Cao, J., Che, H., Chen, J., Ding, A., Fu, P., Gao, J., Gao, Y., Ge, M., Ge, X., Han, Z., He, H., Huang, R.-J., Huang, X., Liao, H., Liu, C., Liu, H., Liu, J., Liu, S. C., Lu, K., Ma, Q., Nie, W., Shao, M., Song, Y., Sun, Y., Tang, X., Wang, T., Wang, T., Wang, W., Wang, X., Wang, Z., Yin, Y., Zhang, Q., Zhang, W., Zhang, Y., Zhang, Y., Zhao, Y., Zheng, M., Zhu, B., and Zhu, J.: Recent Progress in Atmospheric Chemistry Research in China: Establishing a Theoretical Framework for the “Air Pollution Complex”※, Adv. Atmos. Sci., 1339–1361, 2023.